

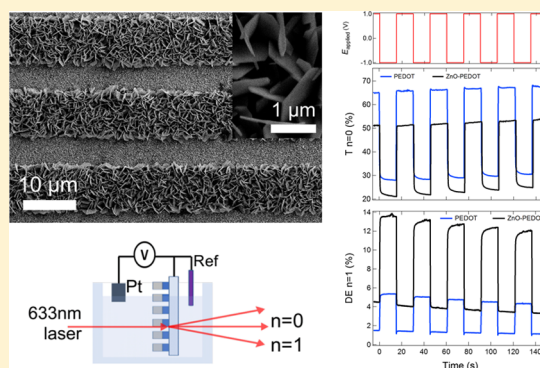
Quantitative Characterization of Optical Coupling in Nanoporous ZnO–WO₃ and ZnO–PEDOT Composite Electrodeposited Gratings Using Electrodiffractive Measurements

Han Wai Millie Fung,¹ Seulgi So,[†] Kellen Kartub, and Robert M. Corn*¹

Department of Chemistry, University of California, Irvine, Irvine, California 92697, United States

Supporting Information

ABSTRACT: To quantitatively characterize the optical coupling between ZnO (a high refractive index but nonabsorptive material) and an electrochromic material (either tungsten oxide (WO₃) or poly(3,4-ethylenedioxythiophene) (PEDOT)), electrodiffractive and electrochromic properties were investigated from a novel two-component composite nanostructured electrodeposited grating that incorporated both ZnO and either WO₃ or PEDOT. The sequential electrodeposition of these two materials through a photopatterned photoresist layer onto a fluorine-doped tin oxide (FTO)-coated glass substrate created a grating structure that exhibited optical diffraction that could be modulated electrochemically. SEM images of the electrochromic gratings revealed that the ZnO electrodeposition created a high surface area nanostructured thin film. The nanostructured ZnO is nonabsorbing, but its high refractive index and large surface area redirect light into the electrochromic grating and create a 4-fold enhancement in the grating's electrodiffractive response.



INTRODUCTION

Zinc oxide's (ZnO) well-documented optical properties have been utilized for a variety of light-based applications. For example, its wide band gap (3.37 eV) has made ZnO a popular semiconductor material for photosensitized dyes with enhanced photovoltaic efficiency.^{1–3} In addition to its semiconductor capabilities, ZnO has been observed to enhance the optical properties within various systems. ZnO was reported to improve the light trapping capabilities of solar cells both as a thin film on an absorbing material⁴ and as a nanopatterned surface.^{5,6} Within our lab, we observed that ZnO nanostructures used in a hierarchical fashion on Au and PEDOT nanocone array surfaces enhanced the antireflective properties of the nanocone arrays via optical coupling.⁷ This is striking because while ZnO has no absorptive properties itself, it seemed to enhance those of the host material beneath. To further our understanding of the optical enhancement of ZnO, we extend our previous work on ZnO nanocone arrays and turn to optical diffraction gratings made of composite electrodeposited ZnO and electrochromic WO₃ or PEDOT to quantify the optical coupling effects.

Optical diffraction gratings that split, redirect, and disperse light are fundamental optical elements that have been incorporated into a myriad of optical devices including laser barcode scanners, optical switches, and spectrometers.^{8–16} Their simple design only requires a surface or thin film material with an optical response that varies periodically on the order of the wavelength of light to exhibit optical diffraction. If we define the linear optical response in terms of the complex

refractive index $n = \eta + i\kappa$, then periodic variations in κ are typically called absorptive gratings, while periodic variations in η are described as phase gratings.^{17–23} Within our own system, ZnO is known to have a large η value ($\eta = 1.998$ at 633 nm), but no κ . Therefore, we theorize that any changes observed in κ in the presence of ZnO must be due to coupling of the ZnO with the absorptive components within the gratings.

To probe the absorptive effects (κ) in addition to the refractive effects (η) of our optical gratings, electrochromic materials were selected as an absorptive host material. Electrochromic thin films are a unique class of materials with a complex refractive index that can be varied reversibly by either oxidation or reduction reactions induced by changes in an applied potential in an electrochemical cell. The electrochromism of these thin films specifically refers to the electrochemically induced color changes. Considering that any changes to the absorptive properties of a material implies a change to the imaginary part of the refractive index, electrochromic thin films demonstrate a potential dependence of κ ; however, changes in η , the real part of the complex refractive index, can also occur. Two of the most well-studied electrodeposited electrochromic thin film materials are tungsten oxide (WO₃)^{24–27} and poly(3,4-ethylenedioxythiophene) (PEDOT).^{28–32} Typical potential-dependent variations of κ for these two materials are ± 0.09 and ± 0.07 ,

Received: August 19, 2018

Revised: November 5, 2018

Published: December 6, 2018

respectively, in the visible region at 600 nm.^{33,34} Because of the potential dependence of η and κ for electrochromic thin films, diffraction gratings that are fabricated from these materials also exhibit a diffraction efficiency that varies with applied potential. This effect has been observed previously and has been denoted either as “electrochemically modulated diffraction”^{22,35–37} or “electrotunable diffraction”,^{38,39} but in this paper, we will denote this phenomenon simply as “electrodiffractive”.

In this article, we have observed and quantified the enhancement of electrodiffractive from a novel two-component composite nanostructured diffraction grating that incorporates both an electrochromic material (either WO_3 or PEDOT) and a nanostructured high refractive index ZnO ($n = 1.998$ at 633 nm). These composite gratings are fabricated by a two-step electrodeposition process on a fluorine-doped tin oxide (FTO)-coated glass substrate as depicted schematically in Figure 1. A pattern of 10 μm wide lines of either WO_3 or

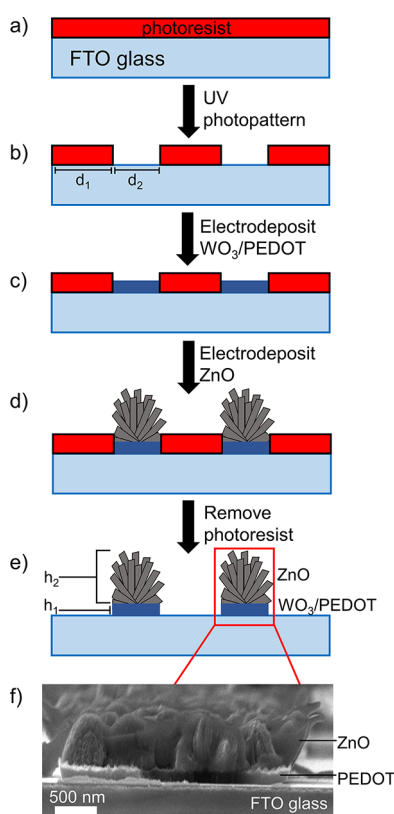


Figure 1. Schematic of the fabrication process of ZnO– WO_3 and ZnO–PEDOT gratings shown in (a–e). A cross-sectional SEM image (f) reveals the various components of a sample ZnO–PEDOT grating.

PEDOT separated by 5 μm of glass is created by electrodeposition onto an FTO glass substrate that is partially protected with a photopatterned film of photoresist. This initial electrochromic grating pattern has a film thickness of ~ 200 nm. A second electrodeposition step creates a nanostructured ZnO film on top of the electrochromic grating, with a film thickness of typically 600 nm. We show that this nonabsorbing nanostructured ZnO film enhances both the optical absorption and the electrodiffractive from this grating; the optical coupling between ZnO and the electrochromic host material results in a 4-fold increase of the electrodiffractive response.

EXPERIMENTAL CONSIDERATIONS

Fabrication of WO_3 Gratings. FTO-coated glass slides ($\sim 30 \Omega/\text{sq cm}$, Sigma-Aldrich) were cleaned by ultrasonication in an aqueous Hellmanex (1%) solution, rinsed with deionized water and ethanol, and dried under an N_2 stream. The FTO-coated glass slides were then plasma cleaned under O_2 plasma for 2 min. The S1808 positive photoresist was spin-coated at 2500 rpm for 80 s onto the glass slides, baked at 90 $^\circ\text{C}$ for 25 min to evaporate photoresist solvent, and cooled to room temperature. The photoresist-coated glass slides were exposed to a UV lamp source (50 W, Oriel Instruments He (Xe) arc lamp) for 3.5 s and patterned using a photomask with 5 μm wide Cr lines and 10 μm glass spacings. The photoresist was then developed for 25 s using an MF-319 developer (Microchem), rinsed with deionized water, and dried under an N_2 stream. An electrical contact area was made by dissolving the corner of the photoresist with acetone using a Q-tip. WO_3 was then electrochemically deposited onto the photopatterned FTO substrate using a potentiostat (PGSTAT12, Metrohm Autolab) in a three-electrode setup. The working electrode of the photopatterned FTO substrate was exposed to an aqueous peroxotungstic acid ($\text{H}_2\text{W}_2\text{O}_{11}$) plating solution for 150 s at a cathodic potential of -0.5 V vs a Ag/AgCl reference electrode in the presence of a Pt counter electrode.

Fabrication of PEDOT Gratings. FTO glass slides ($\sim 30 \Omega/\text{sq cm}$, Sigma-Aldrich) were degreased by sonication in deionized water, acetone, and methanol and then dried with a nitrogen jet. Poly(3,4-ethylenedioxythiophene)–poly(styrenesulfonate) (PEDOT:PSS, 2.0 wt % in H_2O , Sigma-Aldrich) was mixed with isopropyl alcohol and ethylene glycol (ratio 85:10:5) to enhance electronic conductivity and improve wetting. A thin PEDOT:PSS layer was spin-coated onto the FTO glass substrate at 3000 rpm for 20 s. Positive photoresist (S1808, Microchem) was then spin-coated at 2500 rpm for 80 s onto the FTO glass substrate and baked at 90 $^\circ\text{C}$ for 25 min to evaporate the photoresist solvent. After cooling to room temperature, the photomask with 5 μm wide Cr lines and 10 μm glass spacings was placed flushed onto the substrate. The photoresist was exposed through the photomask using a UV lamp source (50 W, Oriel Instruments He (Xe) arc lamp) for 3.5 s. The photoresist was patterned and developed with an MF-319 developer, rinsed with deionized water, and dried under a N_2 stream. An electrical contact area was made by dissolving the corner of the photoresist with acetone using a Q-tip. The PEDOT electrodeposition was performed with a potentiostat (PGSTAT12, Metrohm Autolab), where the FTO glass substrate was exposed to an aqueous electrolyte consisted with 0.02 M 3,4-ethylenedioxythiophene (EDOT, 97%, Sigma-Aldrich), 0.1 M sodium dodecyl sulfate (SDS), and 0.1 M lithium perchlorate (LiClO_4 , 99.5%, Alfa) at a constant potential of +1.0 V vs a Ag/AgCl reference electrode for 45 s in the presence of a Pt counter electrode.

Fabrication of Nanostructured ZnO Gratings. The electrodeposition of nanostructured ZnO was performed with a potentiostat (PGSTAT12, Metrohm Autolab) using a three-electrode setup. An aqueous solution containing 0.1 M $\text{Zn}(\text{NO}_3)_2 \cdot 6\text{H}_2\text{O}$ (98%, Sigma-Aldrich) and 0.1 M KCl heated to 70 $^\circ\text{C}$ was used as the plating solution. The working electrode of either a WO_3 or PEDOT grating array surface was exposed to the plating solution for 600 s at a constant potential of -0.9 V vs a Ag/AgCl reference electrode and in the

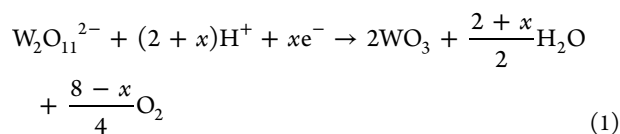
presence of a Pt counter electrode to form a nanostructured ZnO film over the WO₃ or PEDOT gratings. Finally, the sample was rinsed with acetone to remove remaining photoresist and dried under a N₂ stream.

Morphological Characterization. SEM images were obtained using a FEI Magellan 400 field-emission scanning electron microscope at an accelerating voltage of 5 kV. AFM measurements were collected using an Asylum Research MFP-3D, and AFM images were analyzed using Gwyddion imaging processing software. XPS measurements were collected using a Kratos Analytical AXIS Supra surface analysis instrument, with an emission current of 15 mA during analysis. For UV–vis/NIR absorbance measurements, a Jasco V-670 UV–vis/NIR spectrophotometer was used. To measure *ex situ* absorbance spectra, a potential of –1.0 V vs Ag/AgCl was applied to the grating surfaces for 30 s in a 0.1 M LiClO₄ in polycarbonate solution before removing the grating surfaces from solution for spectroscopic analysis. To measure *in situ* absorbance spectra, UV–vis/NIR measurements were collected while a potential of –1.0 V vs Ag/AgCl was applied to the grating surfaces in a 0.1 M LiClO₄ in polycarbonate solution.

Optical Diffraction Analysis. For diffraction and transmittance measurements, the grating surface was placed in an electrochemical cell connected to a potentiostat (Palmsens3, Palmsens) in a three-electrode setup. The grating sample was placed in a 0.1 M LiClO₄ in polycarbonate solution under alternating step potentials of –1.0 and +1.0 V (15 s at each potential for a total duration of 250 s) vs a Ag/AgCl reference electrode and in the presence of a Pt counter electrode. Light from a HeNe laser ($\lambda = 633$ nm, 12 mW, LHRP-1201, Research Electro-Optics), p-polarized using a polarizer (Newport), was emitted and chopped at a frequency of 1.0 kHz using an optical chopper (Stanford Research Instruments SR540). A transmission geometry was employed in these optical measurements, where the intensities of the diffracted light (at the $n = 1$ spot) and transmitted light (at the $n = 0$ spot) were measured by a photodiode (Hamamatsu) connected to a DSP lock-in amplifier (EG&G model 7220). The photodiode potentials were recorded by a Labview program. For %T measurements at the $n = 0$ spot, a FTO glass substrate was used as reference. For %DE measurements, the photodiode intensities at the $n = 1$ spot were divided by the photodiode intensity at the $n = 0$ spot at +1.0 V vs Ag/AgCl (when the grating is at its most transmissive state).

RESULTS AND DISCUSSION

Electrodeposition and Characterization of ZnO–WO₃ and ZnO–PEDOT Gratings. *WO₃ Electrodeposition.* The mechanism of WO₃ electrodeposition from acidic peroxytungstic acid (H₂W₂O₁₁) solutions has been described previously by other researchers.^{40,41} Electrodeposition occurred at negative potentials (–0.4 V vs Ag/AgCl for 150 s) through a combination of electrochemical reduction and disproportionation of the four peroxide (O₂^{2–}) anions in the peroxytungstate ions as described in eq 1, where x is either 0, 4, or 8:



If $x = 8$, then all four of the peroxide anions are reduced electrochemically to three O^{2–} ions (in the electrodeposited

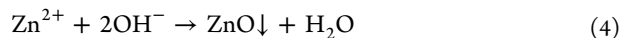
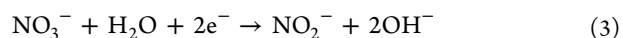
WO₃) and five H₂O. If $x = 0$, then the four peroxide anions disproportionate to form three O^{2–} ions, H₂O, and two O₂. In addition to the peroxide reduction, a nonstoichiometric amount of W⁶⁺ ions in the WO₃ are also reduced to W⁵⁺:



This tungsten reduction is verified by the observation of a blue color of the electrodeposited WO₃ film.

PEDOT Electrodeposition. A PEDOT film was formed by the electrodeposition of 3,4-ethylenedioxythiophene (EDOT) using a slightly modified procedure of a previously reported method.^{42–45} To generate stable, uniform PEDOT films, it was necessary to first spin-coat a thin layer of PEDOT:PSS solution onto the FTO glass substrate to enhance conductivity and improve wetting of the surface, followed by the electropolymerization of EDOT to form a thicker layer of PEDOT. For the electrodeposition, an aqueous plating solution consisting of 0.02 M EDOT, 0.1 M SDS, and 0.1 M LiClO₄ was employed. A constant potential of +1.0 V vs Ag/AgCl was applied for 45 s to a photopatterned FTO glass substrate in the presence of a Pt counter electrode, creating a large-scale (on the cm² scale) uniform electroactive film. The electrodeposited film is in the reduced state, as evidenced by its blue color.

ZnO Electrodeposition. Nanostructured ZnO was selectively deposited electrochemically on top of the WO₃ or PEDOT thin film. In our approach, 0.1 M aqueous zinc nitrate at pH 4.0 heated to 70 °C was used as the plating solution, and electrodeposition occurred for 600 s at a potential of –0.9 V vs Ag/AgCl to ensure full coverage of ZnO over WO₃ or PEDOT gratings. An SEM image of a ZnO–PEDOT grating sample with a ZnO electrodeposition time of 300 s, as shown in the Supporting Information (Figure S1), revealed sparse coverage of ZnO on the grating surface. The mechanism of the ZnO electrodeposition process has been discussed in previous works^{7,46,47} and is summarized as follows: At a sufficiently negative applied potential, OH[–] ions are generated, likely via the reduction of NO₃[–] (eq 3). The OH[–] and the Zn²⁺ ions then result in the precipitation of ZnO onto the working electrode of either WO₃ or PEDOT gratings (eq 4).



Grating Fabrication. The ZnO–WO₃ and ZnO–PEDOT gratings were fabricated using a combination of photolithography and electrodeposition. As shown in the scheme in Figure 1, after a layer of photoresist was spin-coated onto conductive FTO glass slides, UV photopatterning was employed to create an array of photoresist stripes of width $d_1 = 5$ μm that were separated by 10 μm spacings of glass substrate. WO₃ or PEDOT was then selectively deposited electrochemically onto the exposed glass to form arrays of continuous micrometer-scale stripes of width $d_2 = 10$ μm . After the electrodeposition of both the electrochromic and ZnO layers, the photoresist was removed using acetone to create a diffraction grating surface that consists of an array of 10 μm wide ZnO–WO₃ or ZnO–PEDOT stripes separated by 5 μm wide spacings. The morphology of the ZnO–WO₃ and ZnO–PEDOT diffraction gratings was characterized using a combination of SEM, AFM, and XPS. A cross-sectional SEM image in Figure 1f shows the various components of a sample composite ZnO–PEDOT grating, while SEM images in Figure 2 show (a) ZnO–WO₃ gratings and (b) ZnO–PEDOT

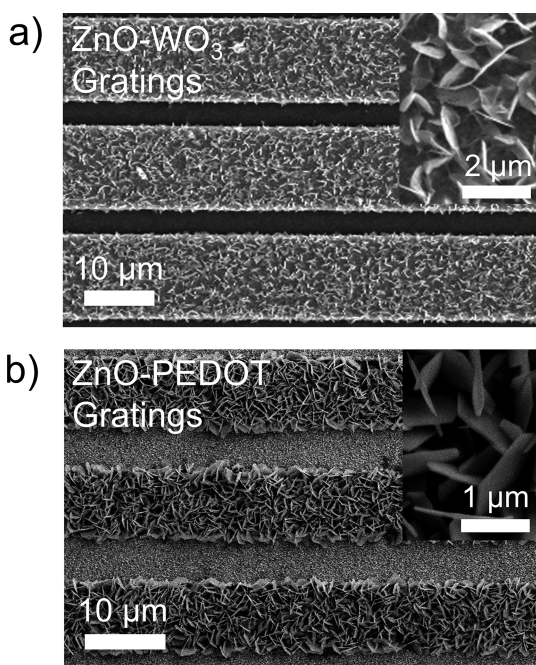


Figure 2. SEM images of a set of (a) ZnO–WO₃ and (b) ZnO–PEDOT gratings. The insets show high-resolution images of the nanostructured ZnO overlayer decorating the gratings.

gratings that are composed of an array of 10 μm wide stripes that extend continuously over a length of several micrometers with 5 μm spacings in between. It should also be noted that the lower contrast in Figure 2b compared to Figure 2a is due to the presence of a thin layer of PEDOT:PSS in the 5 μm spacings between the ZnO–PEDOT stripes in the ZnO–PEDOT gratings (since a thin layer of PEDOT:PSS was spin-coated onto the FTO glass substrate to ensure stable electro-polymerized PEDOT thin films), whereas the ZnO–WO₃ stripes are separated by 5 μm spacings of glass substrates in the ZnO–WO₃ gratings. The insets of the SEM images show high-resolution images of the nanostructured ZnO, where the individual flakelike ZnO nanostructures on the surface are depicted. This is a contrast to the mostly planar and featureless morphology of the WO₃ or PEDOT gratings before the addition of the ZnO layer, as confirmed by SEM images in Figure S2. In addition, AFM measurements (see Figure S3) reveal that an electrochromic layer of height $h_1 = 200$ nm was formed and a nanostructured ZnO layer of height $h_2 = 600$ nm was formed. Furthermore, XPS measurements confirmed the formation of ZnO over both the WO₃ and PEDOT grating surfaces (Figure S4).

Absorbance Spectra of ZnO–WO₃ and ZnO–PEDOT Gratings. The absorbance spectra of the composite gratings were measured using a normal incidence transmission geometry, and it was revealed that the addition of a nanostructured ZnO overlayer on both the WO₃ and PEDOT gratings resulted in enhanced light absorption capabilities. The UV–vis/NIR absorbance spectra for an electrodeposited WO₃ thin film (blue curve), an electrodeposited WO₃ grating (red curve), and an electrodeposited composite ZnO–WO₃ grating (black curve) are all shown in Figure 3a. These three *ex situ* spectra were obtained from samples that were first held at an applied potential of –1.0 V vs Ag/AgCl for 30 s in an electrochemical cell containing a 0.1 M LiClO₄ solution and then removed for spectroscopic measure-

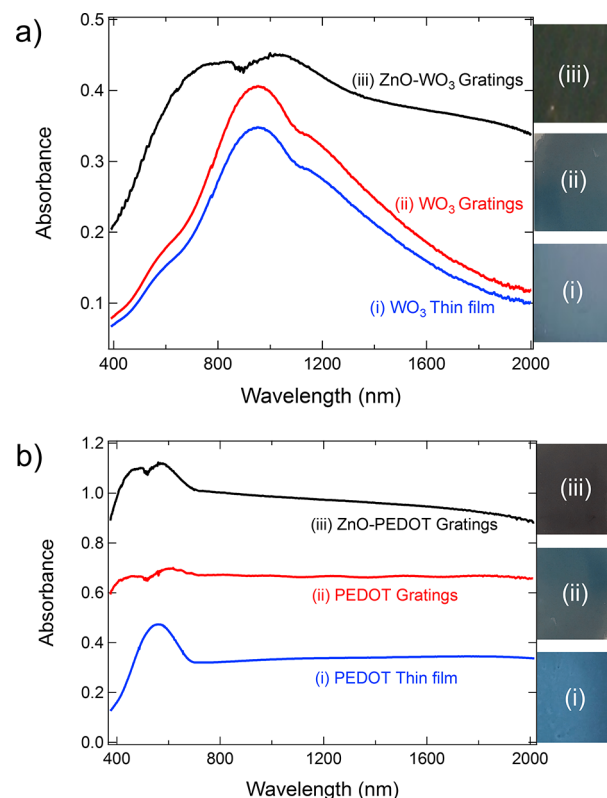


Figure 3. (a) UV–vis/NIR spectra of ZnO–WO₃ gratings, WO₃ gratings, and WO₃ thin film. (b) UV–vis/NIR spectra of ZnO–PEDOT gratings, PEDOT gratings, and PEDOT thin film. Photographs of each sample are also shown.

ments. Absorbance measurements were presented *ex situ* since the spectral changes for our samples were greatest when measurements were performed in air. *In situ* measurements in LiClO₄ solution were also taken to confirm that the absorbance spectra displayed similar visual qualities, as shown in Figure S5. As seen in Figure 3a, there is a strong absorbance peak around 1000 nm for both the planar WO₃ thin films and the WO₃ gratings. Photographs of these two surfaces are also shown in Figure 3a, and both exhibit the well-known blue color associated with reduced WO₃ electrochromic films. The spectrum of the WO₃ grating shows a slightly stronger absorption band than the planar thin film, and thus the color of the WO₃ grating is a darker blue.

In contrast, the spectrum of the ZnO–WO₃ grating shows significantly enhanced absorbance at all wavelengths from 400 to 2000 nm. The addition of the nanostructured ZnO overlayer must enhance the light absorption capabilities of the WO₃ grating underneath, since the electrodeposited ZnO has a high refractive index but no absorptive component ($\kappa = 0$). The UV–vis/NIR absorbance spectrum of ZnO does not exhibit any absorption bands from 400 to 2000 nm due to its high bandgap of 3.3 eV (375 nm).⁴⁸ Nevertheless, the addition of ZnO to form the ZnO–WO₃ gratings significantly enhances the optical absorption of the WO₃ gratings. The enhanced absorption also results in changes in visual appearance of the ZnO–WO₃ gratings, which becomes black as shown in Figure 3a. This data clearly shows that there is a significant amount of light coupled or redirected from the nanostructured ZnO overlayer to the underlying WO₃ portion of the grating structure.

A similar effect was observed for ZnO–PEDOT gratings. The UV–vis/NIR absorbance spectra of an electrodeposited planar PEDOT thin film, an electrodeposited PEDOT grating, and an electrodeposited ZnO–PEDOT grating are shown in Figure 3b. It has been shown previously that PEDOT thin films exhibit a π -to- π^* transition with a band gap of 1.7 eV (775 nm); thus, PEDOT thin films in the reduced state show significant optical absorption near 600 nm,^{31,32,49} as evidenced by the blue trace in Figure 3b. Similar to the WO₃, PEDOT films also have a characteristic blue color in the reduced state as seen in the inset to Figure 3b. The PEDOT grating adds an additional absorption band at 450 nm (see Figure 3b) that has been attributed to an interference effect of the PEDOT grating and is a darker blue in color as seen in the Figure 3b inset. As in the case of the ZnO–WO₃ gratings, the ZnO–PEDOT gratings also show a broadband enhancement in the UV–vis/NIR absorbance spectrum and have a black visual appearance, also seen in the inset of Figure 3b. We attribute this enhanced absorption from of ZnO–PEDOT gratings to the same mechanism as in the of ZnO–WO₃ gratings: coupling or redirection of light from the nanostructured ZnO overlayer to the underlying PEDOT grating.

Electrodiffractive of ZnO–WO₃ and ZnO–PEDOT Gratings. While the nanostructured ZnO overlayer enhances the absorptive properties of WO₃ and PEDOT gratings, there is an even larger effect on the electrochemically modulated diffraction. Electrodiffraction from electrodeposited ZnO–WO₃ and ZnO–PEDOT gratings at $\lambda = 633$ nm was measured *in situ* at normal incidence in an electrochemical cell containing 0.1 M LiClO₄ in polycarbonate, as shown schematically in Figure 4a. A representative diffraction pattern is shown in Figure 4b.

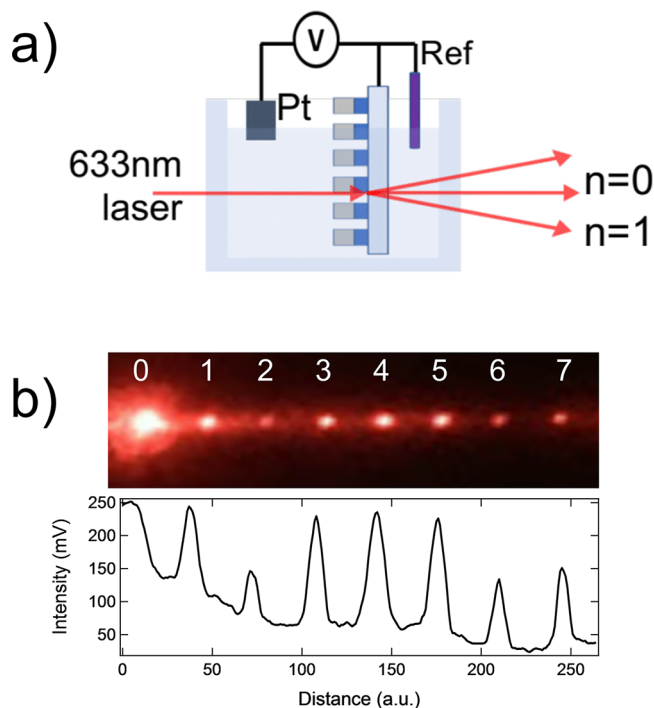


Figure 4. (a) Schematic of the setup used for electrochemically modulated optical measurements of ZnO–WO₃ and ZnO–PEDOT gratings. (b) Photograph of and intensity profile of diffraction pattern created by a set of ZnO–WO₃ gratings.

To measure the electrodiffraction and electrochromic response, the applied potential to a ZnO–WO₃ or ZnO–PEDOT grating was stepped between -1.0 and $+1.0$ V vs Ag/AgCl every 15 s. The current transients from the potential steps are shown in Figure 5. The current transients are higher

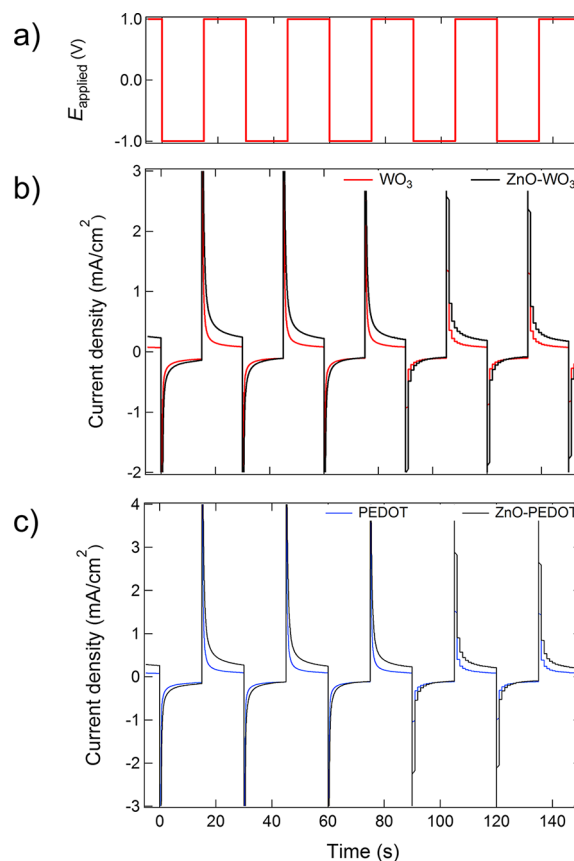


Figure 5. (a) For the applied step potentials of -1.0 and $+1.0$ V vs Ag/AgCl, corresponding current transients for (b) ZnO–WO₃ and WO₃ gratings as well as (c) ZnO–PEDOT and PEDOT gratings are shown.

for the ZnO–WO₃ grating as compared to the WO₃ grating, as shown in Figure 5b; we attribute this to the larger charging currents for high surface area nanostructured ZnO. Similar trends were observed for the ZnO–PEDOT and PEDOT gratings in Figure 5c.

The electrochemically modulated optical signals for electrochromic changes (transmission at $n = 0$) and first-order diffraction ($n = 1$) were acquired as a function of time from both ZnO–WO₃ gratings (Figures 6b and 6c) and ZnO–PEDOT gratings (Figures 7b and 7c). Transmission measurements at $n = 0$ were collected *in situ* at normal incidence at $\lambda = 633$ nm in an electrochemical cell containing 0.1 M LiClO₄ in polycarbonate using a FTO-coated glass slide as reference. To ensure reproducibility, optical measurements were acquired as the applied potentials were stepped between $+1.0$ and -1.0 V (potentials measured against Ag/AgCl) for a total of 10 times. The %T observed in Figure 6b from the $n = 0$ spot for both WO₃ gratings and ZnO–WO₃ gratings varied reversibly with the applied potential as a result of the electrochromic properties of WO₃. For the WO₃ grating, %T switched between 79% at $+1.0$ V and 27% at -1.0 V vs Ag/AgCl. This variation in %T is indicative of the electrochromic effects

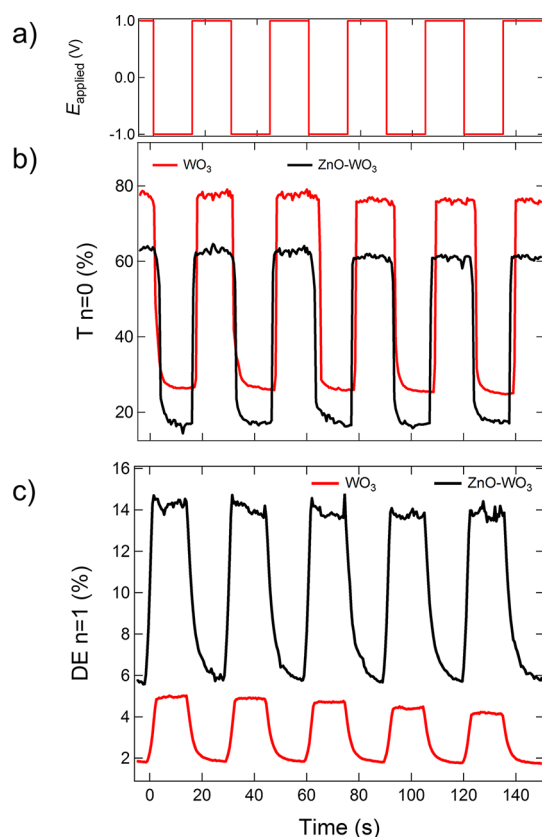


Figure 6. Optical measurements of ZnO–WO₃ and WO₃ gratings after (a) applied potentials of –1.0 V and +1.0 V vs Ag/AgCl showing the (b) transmittance at the $n = 0$ spot and the (c) diffraction efficiency at the $n = 1$ spot.

displayed by the WO₃ grating, with larger $\Delta\%T$ values indicating a greater optical contrast under an applied potential. At –1.0 V, Li ion intercalation and electron injection into the WO₃ grating lead to an increase in κ and thus the large increase ($\Delta\%T = 52\%$) in light absorption. This effect has been observed previously on both planar WO₃ films and gratings.^{24–26} Similar electrochromic effects were observed for the ZnO–WO₃ gratings, with a $\Delta\%T = 46\%$. However, the average intensity of the transmitted light was lower for the ZnO–WO₃ gratings as compared to undecorated WO₃ gratings ($T_{\text{ave}} = 40\%$ vs $T_{\text{ave}} = 55\%$). This decrease is expected from the absorption spectra results discussed in the previous section.

Then, for electrodiffraction experiments, optical measurements were also collected *in situ* at normal incidence at $\lambda = 633$ nm in an electrochemical cell containing 0.1 M LiClO₄ in polycarbonate using the gratings' $n = 0$ transmission measurements at +1.0 V vs Ag/AgCl (the gratings' most transmissive state) as reference. To ensure reproducibility, %DE measurements were reported as the applied potentials were stepped between +1.0 and –1.0 V (potentials measured against Ag/AgCl) for a total of 10 times. In contrast to the electrochromic behavior, both the average and the electrochemically modulated diffraction efficiency (%DE) observed for the $n = 1$ diffraction spot were greater for the ZnO–WO₃ gratings compared to the WO₃ gratings. It should also be noted that the electrochemical modulation of %DE was 180° out of phase with the modulation of %T. A comparison of Figures 6b and 6c revealed that the more absorptive state at $n = 0$ (for the applied

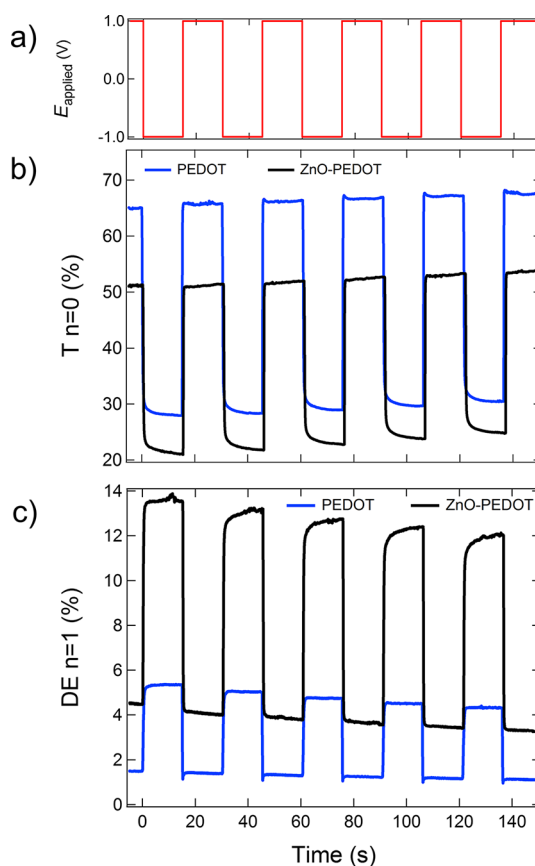


Figure 7. Optical measurements of ZnO–PEDOT and PEDOT gratings after (a) applied potentials of –1.0 V and +1.0 V vs Ag/AgCl showing the (b) transmittance at the $n = 0$ spot and the (c) diffraction efficiency at the $n = 1$ spot.

potential –1.0 V vs Ag/AgCl) displayed a low %T but a high %DE, and vice versa at +1.0 V vs Ag/AgCl. From the red trace in Figure 6c, an average %DE of 3.2% and an electrochemically modulated $\Delta\%DE$ of 2.4% were observed for WO₃ gratings. As for the ZnO–WO₃ gratings (black trace in Figure 6c), the average %DE increased to 10%, and the electrodiffraction increased to a $\Delta\%DE$ of 9.7%—4 times higher than the gratings without ZnO. A similar effect was observed for the case of the ZnO–PEDOT and PEDOT gratings. As seen in Figure 7b, for PEDOT gratings %T and $\Delta\%T$ were 45% and 35%, respectively; these values decreased to 36% and 27% for ZnO–PEDOT gratings. However, the diffraction efficiencies again showed significant increases: an average %DE and $\Delta\%DE$ were 3.5% and 2.8% for PEDOT gratings but increased significantly to 8.5% and 8.3%, respectively, as shown in Figure 6c. The drastic increase of $\Delta\%DE$ displayed by the ZnO–WO₃ and ZnO–PEDOT gratings compared to their counterpart WO₃ and PEDOT gratings indicates a significant improvement of their electrodiffraction performance, likely due to optical coupling between ZnO and the host material. By reporting $\Delta\%DE$ values, we have demonstrated that we can quantify optical coupling between the nonabsorptive nanostructured ZnO overlayer and the absorptive host material (WO₃ and PEDOT).

To understand these changes in the average %DE and $\Delta\%DE$, we need to consider the contributions to η and κ for the composite gratings. In the case of thin gratings, the diffraction

efficiency (DE) is a linear combination of an absorptive component and a phase component (eq 5):^{22,38,50}

$$DE = a(\Delta\kappa)^2 + b(\Delta\eta)^2 \quad (5)$$

This equation can be used to explain the increases in the average %DE but not the electrodiffraction component ($\Delta\%DE$). For the case of the composite ZnO–WO₃ and ZnO–PEDOT gratings in this paper, an additional coupling between the ZnO and the absorptive WO₃ or PEDOT is observed, even though no electrodiffraction effect ($\Delta\kappa = \Delta\eta = 0$) is observed with ZnO gratings alone (optical measurements shown in Figure S6). Instead, the nanostructured ZnO overlayer redirects light into the electrochromic WO₃ or PEDOT component of the grating. This type of optical coupling occurs because the electrodeposited nanostructured ZnO coating is on the same scale as the light; similar optical effects have been previously observed in calculations of the diffraction efficiency of taller gratings.^{35,50} Furthermore, the high surface area, nanostructured nature of the ZnO provides an additional coupling mechanism via a series of total internal reflection from the ZnO to the absorptive material underneath.⁶ To support our proposed mechanism for optical coupling, we showed that ZnO–PEDOT gratings without a fully covered ZnO overlayer displayed much weaker electrodiffraction effects (see Figure S7). ZnO–PEDOT gratings with a sparse ZnO overlayer only displayed a 1.5-fold enhancement of $\Delta\%DE$ compared to PEDOT gratings, which indicates weaker optical coupling between the sparse ZnO overlayer and the absorptive material underneath. Thus, the presence of the electrodeposited ZnO, in a combination of the nanoscale structure and metamaterial patterning, is crucial for creating enhanced electrodiffraction.

CONCLUSIONS

The enhanced absorption and electrodiffraction observed from the composite ZnO–WO₃ and ZnO–PEDOT gratings described in this paper clearly demonstrate that there is a strong optical coupling between the electrodeposited nanostructured ZnO overlayer and the electrochromic thin film layer underneath. This coupling has some significant implications; the presence of both nanoscale structuring and metamaterial patterning (e.g., gratings, nancone arrays, or nanoring arrays) is required for this coupling to occur. The electrodiffraction from these gratings increases in the presence of the high surface area nanostructured ZnO, even though the ZnO itself has no absorptive (κ) or electrochromic ($\Delta\kappa$) behavior. In these gratings, the ZnO enhances the delivery of light to the underlying electrochromic materials via optical coupling. We have also observed this coupling effect previously in the enhanced antireflectivity of PEDOT and gold nancone arrays that were coated with electrodeposited ZnO nanostructures.⁷ Going forward, we should be able to employ this coupling effect to enhance the production of electron–hole pairs by enhancing the optical absorption of TiO₂, In₂O₃, or Si semiconductor patterned gratings, nancone arrays, or nanoring arrays.

ASSOCIATED CONTENT

Supporting Information

The Supporting Information is available free of charge on the ACS Publications website at DOI: 10.1021/acs.jpcc.8b08072.

SEM images of sparsely ZnO-covered ZnO–PEDOT gratings after applying a ZnO electrodeposition time of 300 s, SEM images of WO₃ and PEDOT gratings, AFM measurements of ZnO-coated gratings, XPS of ZnO-coated gratings, absorbance spectra of ZnO–PEDOT and PEDOT gratings performed *in situ*, optical measurements for the transmission and diffraction efficiency of ZnO only gratings, and optical measurements for the transmission and diffraction efficiency of ZnO–PEDOT gratings with a sparse ZnO overlayer (PDF)

AUTHOR INFORMATION

Corresponding Author

*(R.M.C.) E-mail rcorn@uci.edu.

ORCID

Han Wai Millie Fung: 0000-0003-0667-4113

Robert M. Corn: 0000-0002-4756-2161

Present Address

[†]POSCO Technical Research Laboratories 8, Pockposarangil, Gwangyang-si, Jeollanam-do, 57807, Korea

Notes

The authors declare no competing financial interest.

ACKNOWLEDGMENTS

This work was supported by the National Science Foundation through Grant CHE-1403506. SEM and XPS analyses were performed at the Irvine Materials Research Institute (IMRI) at UC Irvine. UV–vis/NIR measurements were performed at the UC Irvine Laser Spectroscopy Laboratories. The authors thank the Penner Group for their help with AFM measurements.

REFERENCES

- (1) Murakoshi, K.; Yanagida, S.; Capel, M.; Castner, E. W. Interfacial Electron Transfer Dynamics of Photosensitized Zinc Oxide Nanoclusters. In *Nanostructured Materials*; American Chemical Society: 1997; Vol. 679, pp 221–238.
- (2) Conradt, J.; Sartor, J.; Thiele, C.; Maier-Flaig, F.; Fallert, J.; Kalt, H.; Schneider, R.; Fotouhi, M.; Pfundstein, P.; Zibat, V.; Gerthsen, D. Catalyst-Free Growth of Zinc Oxide Nanorod Arrays on Sputtered Aluminum-Doped Zinc Oxide for Photovoltaic Applications. *J. Phys. Chem. C* **2011**, *115*, 3539–3543.
- (3) Gonzalez-Valls, I.; Lira-Cantu, M. Vertically-Aligned Nanostructures of ZnO for Excitonic Solar Cells: A Review. *Energy Environ. Sci.* **2009**, *2*, 19–34.
- (4) Müller, J.; Rech, B.; Springer, J.; Vanecek, M. TCO and Light Trapping in Silicon Thin Film Solar Cells. *Sol. Energy* **2004**, *77*, 917–930.
- (5) Battaglia, C.; Escarré, J.; Söderström, K.; Charrière, M.; Despeisse, M.; Haug, F.-J.; Ballif, C. Nanomoulding of Transparent Zinc Oxide Electrodes for Efficient Light Trapping in Solar Cells. *Nat. Photonics* **2011**, *5*, 535.
- (6) Lin, A.; Phillips, J. Optimization of Random Diffraction Gratings in Thin-Film Solar Cells using Genetic Algorithms. *Sol. Energy Mater. Sol. Cells* **2008**, *92*, 1689–1696.
- (7) Fung, H. W. M.; So, S.; Kartub, K.; Loget, G.; Corn, R. M. Ultra-Antireflective Electrodeposited Plasmonic and PEDOT Nancone Array Surfaces. *J. Phys. Chem. C* **2017**, *121*, 22377–22383.
- (8) Yaqoob, Z.; Riza, N. A. Passive Optics No-Moving-Parts Barcode Scanners. *IEEE Photonics Technol. Lett.* **2004**, *16*, 954–956.
- (9) Boudoux, C.; Yun, S. H.; Oh, W. Y.; White, W. M.; Ifthimia, N. V.; Shishkov, M.; Bouma, B. E.; Tearney, G. J. Rapid Wavelength-Swept Spectrally Encoded Confocal Microscopy. *Opt. Express* **2005**, *13*, 8214–8221.

- (10) Chen, J.; Bos, P. J.; Vithana, H.; Johnson, D. L. An Electro-Optically Controlled Liquid Crystal Diffraction Grating. *Appl. Phys. Lett.* **1995**, *67*, 2588–2590.
- (11) Glesk, I.; Bock, P. J.; Cheben, P.; Schmid, J. H.; Lapointe, J.; Janz, S. All-Optical Switching using Nonlinear Subwavelength Mach-Zehnder on Silicon. *Opt. Express* **2011**, *19*, 14031–14039.
- (12) Williams, G. V. M.; Do, M. T. T.; Raymond, S. G.; Bhuiyan, M. D. H.; Kay, A. J. Optically Switchable Diffraction Grating in a Photochromic/Polymer Thin Film. *Appl. Opt.* **2015**, *54*, 6882–6886.
- (13) Bousquet, P. *Spectroscopy and Its Instrumentation*; Hilger: London, 1971.
- (14) Palmer, C. *Diffraction Grating Handbook*, 6th ed.; Newport Corporation: New York, 2005.
- (15) Arafat Hossain, M.; Canning, J.; Ast, S.; Cook, K.; Rutledge, P. J.; Jamalipour, A. Combined “Dual” Absorption and Fluorescence Smartphone Spectrometers. *Opt. Lett.* **2015**, *40*, 1737–1740.
- (16) Yang, M.; Wang, H.; Li, M.; He, J.-J. In *SPIE Optical Engineering + Applications, SPIEAn Echelle Diffraction Grating for Imaging Spectrometer*; SPIE Optical Engineering + Applications; SPIE: 2016; p 7.
- (17) Cheben, P.; Bock, P. J.; Schmid, J. H.; Lapointe, J.; Janz, S.; Xu, D.-X.; Densmore, A.; Del age, A.; Lamontagne, B.; Hall, T. J. Refractive Index Engineering with Subwavelength Gratings for Efficient Microphotonic Couplers and Planar Waveguide Multiplexers. *Opt. Lett.* **2010**, *35*, 2526–2528.
- (18) Knop, K. Rigorous Diffraction Theory for Transmission Phase Gratings with Deep Rectangular Grooves. *J. Opt. Soc. Am.* **1978**, *68*, 1206–1210.
- (19) Botten, I. C.; Craig, M. S.; McPhedran, R. C.; Adams, J. L.; Andrewartha, J. R. The Dielectric Lamellar Diffraction Grating. *Opt. Acta* **1981**, *28*, 413–428.
- (20) Kondrachova, L. V.; May, R. A.; Cone, C. W.; Vanden Bout, D. A.; Stevenson, K. J. Evaluation of Lithium Ion Insertion Reactivity via Electrochromic Diffraction-Based Imaging. *Langmuir* **2009**, *25*, 2508–2518.
- (21) Bailey, R. C.; Hupp, J. T. Large-Scale Resonance Amplification of Optical Sensing of Volatile Compounds with Chemoresponsive Visible-Region Diffraction Gratings. *J. Am. Chem. Soc.* **2002**, *124*, 6767–6774.
- (22) Schanze, K. S.; Bergstedt, T. S.; Hauser, B. T.; Cavalaheiro, C. S. P. Photolithographically-Patterned Electroactive Films and Electrochemically Modulated Diffraction Gratings. *Langmuir* **2000**, *16*, 795–810.
- (23) Massari, A. M.; Stevenson, K. J.; Hupp, J. T. Development and Application of Patterned Conducting Polymer Thin Films as Chemoresponsive and Electrochemically Responsive Optical Diffraction Gratings. *J. Electroanal. Chem.* **2001**, *500*, 185–191.
- (24) Mortimer, R. J.; Rosseinsky, D. R.; Monk, P. M. S. *Electrochromic Materials and Devices*, 1st ed.; Wiley-VCH Verlag GmbH & Co. KGaA: Berlin, 2015.
- (25) Mortimer, R. J. *Electrochromic Materials*. *Annu. Rev. Mater. Res.* **2011**, *41*, 241–268.
- (26) Somani, P. R.; Radhakrishnan, S. Electrochromic Materials and Devices: Present and Future. *Mater. Chem. Phys.* **2003**, *77*, 117–133.
- (27) Granqvist, C. G. Electrochromics for Smart Windows: Oxide-Based Thin Films and Devices. *Thin Solid Films* **2014**, *564*, 1–38.
- (28) Kirchmeyer, S.; Elschner, A.; Reuter, K.; Lovenich, W.; Merker, U. *PEDOT: Principles and Applications of an Intrinsically Conductive Polymer*; CRC Press: 2010.
- (29) Sankaran, B.; Reynolds, J. R. High-Contrast Electrochromic Polymers from Alkyl-Derivatized Poly(3,4-ethylenedioxythiophenes). *Macromolecules* **1997**, *30*, 2582–2588.
- (30) Mortimer, R. J. Organic Electrochromic Materials. *Electrochim. Acta* **1999**, *44*, 2971–2981.
- (31) Kumar, A.; Welsh, D. M.; Morvant, M. C.; Piroux, F.; Abboud, K. A.; Reynolds, J. R. Conducting Poly(3,4-alkylenedioxythiophene) Derivatives as Fast Electrochromics with High-Contrast Ratios. *Chem. Mater.* **1998**, *10*, 896–902.
- (32) Ruffo, R.; Celik-Cochet, A.; Posset, U.; Mari, C. M.; Schottner, G. Mechanistic Study of the Redox Process of an *In Situ* Oxidatively Polymerised Poly(3,4-ethylene-dioxythiophene) Film. *Sol. Energy Mater. Sol. Cells* **2008**, *92*, 140–145.
- (33) Von Rottkay, K.; Rubin, M.; Wen, S. J. Optical Indices of Electrochromic Tungsten Oxide. *Thin Solid Films* **1997**, *306*, 10–16.
- (34) Pettersson, L. A. A.; Ghosh, S.; Ingan s, O. Optical Anisotropy in Thin Films of Poly(3,4-ethylenedioxythiophene)-Poly(4-styrenesulfonate). *Org. Electron.* **2002**, *3*, 143–148.
- (35) Dang, X.; Massari, A. M.; Hupp, J. T. Electrochemically Modulated Diffraction - A Novel Strategy for the Determination of Conduction-Band-Edge Energies for Nanocrystalline Thin-Film Semiconductor Electrodes. *Electrochim. Solid-State Lett.* **1999**, *3*, 555–558.
- (36) Kim, Y.; Kim, Y.; Kim, S.; Kim, E. Electrochromic Diffraction from Nanopatterned Poly(3-hexylthiophene). *ACS Nano* **2010**, *4*, 5277–5284.
- (37) Park, C.; Na, J.; Han, M.; Kim, E. Transparent Electrochemical Gratings from a Patterned Bistable Silver Mirror. *ACS Nano* **2017**, *11*, 6977–6984.
- (38) Tian, S.; Armstrong, N. R.; Knoll, W. Electrochemically Tunable Surface-Plasmon-Enhanced Diffraction Gratings and their (Bio-)sensing Applications. *Langmuir* **2005**, *21*, 4656–4660.
- (39) Matsui, T.; Ozaki, M.; Yoshino, K. In *Electro-Tunable Liquid Crystal Waveguide Laser*, Optical Science and Technology, the SPIE 49th Annual Meeting; SPIE: 2004; p 12.
- (40) Meulenkamp, E. A. Mechanism of WO₃ Electrodeposition from Peroxy-Tungstate Solution. *J. Electrochem. Soc.* **1997**, *144*, 1664–1671.
- (41) Cai, G.; Cui, M.; Kumar, V.; Darmawan, P.; Wang, J.; Wang, X.; Lee-Sie Eh, A.; Qian, K.; Lee, P. S. Ultra-Large Optical Modulation of Electrochromic Porous WO₃ Film and the Local Monitoring of Redox Activity. *Chem. Sci.* **2016**, *7*, 1373–1382.
- (42) So, S.; Fung, H. W. M.; Kartub, K.; Maley, A. M.; Corn, R. M. Fabrication of PEDOT Nanocone Arrays with Electrochemically Modulated Broadband Antireflective Properties. *J. Phys. Chem. Lett.* **2017**, *8*, 576–579.
- (43) Randriamahazaka, H.; Sini, G.; Tran Van, F. Electrodeposition Mechanisms and Electrochemical Behavior of Poly(3,4-ethylenedioxythiophene). *J. Phys. Chem. C* **2007**, *111*, 4553–4560.
- (44) Nguyen, V.-Q.; Schaming, D.; Martin, P.; Lacroix, J.-C. Highly Resolved Nanostructured PEDOT on Large Areas by Nanosphere Lithography and Electrodeposition. *ACS Appl. Mater. Interfaces* **2015**, *7*, 21673–21681.
- (45) Donovan, K. C.; Arter, J. A.; Pilolli, R.; Cioffi, N.; Weiss, G. A.; Penner, R. M. Virus-Poly(3,4-ethylenedioxythiophene) Composite Films for Impedance-Based Biosensing. *Anal. Chem.* **2011**, *83*, 2420–2424.
- (46) Illy, B. N.; Cruickshank, A. C.; Schumann, S.; Da Campo, R.; Jones, T. S.; Heutz, S.; McLachlan, M. A.; McComb, D. W.; Riley, D. J.; Ryan, M. P. Electrodeposition of ZnO Layers for Photovoltaic Applications: Controlling Film Thickness and Orientation. *J. Mater. Chem.* **2011**, *21*, 12949–12957.
- (47) Sun, S.; Jiao, S.; Zhang, K.; Wang, D.; Gao, S.; Li, H.; Wang, J.; Yu, Q.; Guo, F.; Zhao, L. Nucleation Effect and Growth Mechanism of ZnO Nanostructures by Electrodeposition from Aqueous Zinc Nitrate Baths. *J. Cryst. Growth* **2012**, *359*, 15–19.
- (48) Xu, L.; Chen, Q.; Xu, D. Hierarchical ZnO Nanostructures Obtained by Electrodeposition. *J. Phys. Chem. C* **2007**, *111*, 11560–11565.
- (49) Deutschmann, T.; Oesterschulze, E. Micro-Structured Electrochromic Device Based on Poly(3,4-ethylenedioxythiophene). *J. Micromech. Microeng.* **2013**, *23*, No. 06S032.
- (50) Nelson, K. A.; Casalegno, R.; Miller, R. J. D.; Fayer, M. D. Laser-Induced Excited State and Ultrasonic Wave Gratings: Amplitude and Phase Grating Contributions to Diffraction. *J. Chem. Phys.* **1982**, *77*, 1144–1152.